Journal of Magnetism and Magnetic Materials 474 (2019) 152–160

Contents lists available at ScienceDirect

Journal of Magnetism and Magnetic Materials

journal homepage: www.elsevier.com/locate/jmmm

Research articles

Single cell magnetometry by magnetophoresis vs. bulk cell suspension magnetometry by SQUID-MPMS – A comparison

Wei Xue[a,b], Lee R. Moore[a], Naruhiko Nakano[c], Jeffrey J. Chalmers[b], Maciej Zborowski[a,*]

[a] Department of Biomedical Engineering, Lerner Research Institute, Cleveland Clinic, 9500 Euclid Avenue, OH 44195, United States
[b] The William G. Lowrie Department of Chemical and Biomolecular Engineering, The Ohio State University, 151 W. Woodruff Avenue, Columbus, OH 43210, United States
[c] Department of Chemistry for Materials, Mie University, Mie, Japan

A B S T R A C T

Paramagnetic constituents of a cell have strong effect on the cell's volume magnetic susceptibility even at low volume fraction because of their high susceptibility relative to that of the diamagnetic cell constituents. The effect can be measured at a single cell level by measuring cell terminal velocity in viscous media using a microscope equipped with a well-defined field and gradient magnet configuration (referred to as magnetophoretic analysis by cell tracking velocimetry, CTV). The sensitivity of such a microscopic-scale magnetometry was compared to that of a reference method of superconducting quantum interference-magnetic properties measurement system (SQUID-MPMS) using a red blood cell (RBC) suspension model. The RBC hemoglobin oxygen saturation determines the hemoglobin molecular magnetic susceptibility (diamagnetic when fully oxygenated, paramagnetic when fully deoxygenated or converted to methemoglobin). The SQUID-MPMS measurements were performed on an average of 5000 RBCs in 20 μL physiological phosphate buffer at room temperature, those by CTV on a single cell track in a mean magnetic field of 1.6 T and mean gradient of 240 T/m, repeated for an average of 1000 tracks per sample. This suggests 5000× higher sensitivity of cell susceptometry by magnetophoretic analysis than by SQUID-MPMS. The magnetophoretic mean RBC magnetic susceptibilities were in the range determined by SQUID-MPMS (lower limit) and theory (upper limit). The ability of magnetophoretic analysis to resolve susceptibility peaks in a mixed cell populations was confirmed for an oxy RBC and met RBC mixture. Magnetophoretic analysis by CTV provides new tool for studies of emergence of paramagnetic reaction products in the cell.

1. Introduction

Magnetic separation has become an indispensable technique in life science because of its unparalleled sensitivity, selectivity and purity for cell separation and that of DNA and RNA [1–5]. The magnetic properties of the biological matter to be separated, with or without magnetic label, are vital for the separator engineering design [6]. With the increased availability of strong rare-earth magnets and improved designs it is possible to magnetically separate unlabeled, weakly paramagnetic cells [7]. We have developed applications that include intraerythrocytic malaria detection [8,9], separation of bacterial spores rich in paramagnetic element manganese (Mn) [10,11], separation of algae genetically modified for elevated expression of ferritin [2], enrichment of mature erythrocytes from hematopoietic cell cultures [12], erythrocyte depletion from whole blood preparations as a type of a "magnetic centrifuge" [13], analysis of interconversion between low-spin and high-spin hemoglobin [14,15], and developed theory of magnetophoresis that links the field-induced cell motion to the intracellular concentration of paramagnetic species [14,16]. Others have developed practical systems for detecting paramagnetic contaminants in food or environmental water [17], demonstrated an atomic-level sensitivity of the magnetic ponderomotive forces to the paramagnetic contribution in the predominantly diamagnetic materials [18], and to measure cell density [19,20].

A rational design of label-free magnetic cell separator requires knowledge of the cell magnetic susceptibility. The low magnetic susceptibility of cells, their small size (in single to tens of micrometers range) and special handling requirements necessary to maintain their viability pose a challenge to the sensitivity of current magnetometer instruments. There are many different analytical techniques available to measure bulk tissue magnetic properties, including Mössbauer spectroscopy [21], nuclear magnetic resonance (NMR) spectroscopy [22], electron paramagnetic resonance (EPR) [23], Gouy balance [24], vibrating sample magnetometry (VSM) [25], and superconducting quantum interference device-magnetic properties measurement system (SQUID-MPMS). NMR imaging (MRI) is a well-established tool in clinical radiology departments [26]). We became interested in SQUID-MPMS as a reference method because it has been used to examine biological samples in the past [4,27,28] and because it is a quantitative analytical method. Its use has been limited to applications to lyophilized samples only, however. In principle, it is capable of accepting liquid samples, such as cell suspensions required for this study, and therefore we set out to develop a protocol for liquid sample SQUID-MPMS measurements (at room temperature) as a part of this study.

* Corresponding author.
E-mail address: zborowm@ccf.org (M. Zborowski).

https://doi.org/10.1016/j.jmmm.2018.10.108
Received 24 June 2018; Received in revised form 9 October 2018; Accepted 22 October 2018
Available online 28 October 2018
0304-8853/

Single cell magnetophoresis, or magnetically-induced cell motion [3,7,29–31] could be used to determine the cell magnetic susceptibility if measured with an accurate microscopic cell tracking camera equipped with high precision magnet producing well-defined magnetic field in the microscope field of view. To evaluate the accuracy of magnetophoresis method, we compared the magnetic susceptibility measurements of various forms of red blood cells (RBCs, including oxygenated RBCs, met-hemoglobin RBCs, and deoxygenated RBCs) with those measured using SQUID-MPMS. The RBCs were chosen for their known, uniform physical parameters including magnetophoretic mobility and magnetic susceptibility [32].

2. Material and methods

2.1. RBC magnetic susceptibility by magnetophoretic analysis

Magnetophoresis method was described previously [33] and the current setup (Mk V) generating the highest mean field and gradient is introduced here. The hyperbolic pole pieces create a magnetic field with horizontal, nearly constant, well-characterized magnetostatic potential energy density gradient within the microscope field of view (FOV), where the glass channel used as the cell suspension container is situated (Fig. 1). The magnet was assembled using neodymium-iron-boron permanent magnet cubes 38.1 mm to the side from a commercial supplier (K&J Magnetics, Inc., Pipersville, PA) and stock, low carbon steel. At steady state motion, the horizontal component of the cell migration is solely driven by the magnetic field. With the aid of a digital camera and computer image analysis software, the velocity of several hundred cells is acquired simultaneously by analyzing individual cell tracks. The viscous drag of the liquid media acting on slowly moving cells follows the Stokes' law and the magnetic susceptibility of cells can be calculated from the dynamic equilibrium of the magnetic and drag forces resulting in the following equations:

$$u_m = \frac{\chi_{RBC} - \chi_{H2O}}{3\pi\eta}\frac{V_{RBC}}{D_{RBC}}S_m = \frac{\chi_{RBC} - \chi_{H2O}}{18\pi\eta}D_{RBC}^2 S_m \quad (1)$$

$$S_m = \frac{d}{dy}\left(\frac{B^2}{2\mu_0}\right) \quad (2)$$

$$\chi_{RBC} = \frac{18\pi\eta}{D_{RBC}^2 S_m}\langle u_m\rangle + \chi_{H2O} \quad (3)$$

where $\langle u_m\rangle$ is the experimentally determined mean horizontal velocity (m/s) of the RBC induced by the predominantly horizontal gradient of the applied magnetic field (Fig. 1c). The magnet extends sufficiently far into the *x*-axis dimension for the field gradient in FOV to be negligible along that direction. Here χ_{RBC}, χ_{H2O} are the volume magnetic susceptibility of cell and water, respectively (SI unit, dimensionless). V_{RBC} is the cell volume (m3), η is the viscosity of water (Pa·s), D_{RBC} is the equivalent hydrodynamic sphere diameter of the cell (m), S_m is the magnetic energy density gradient (T-A/m^2), B is the local magnetic field

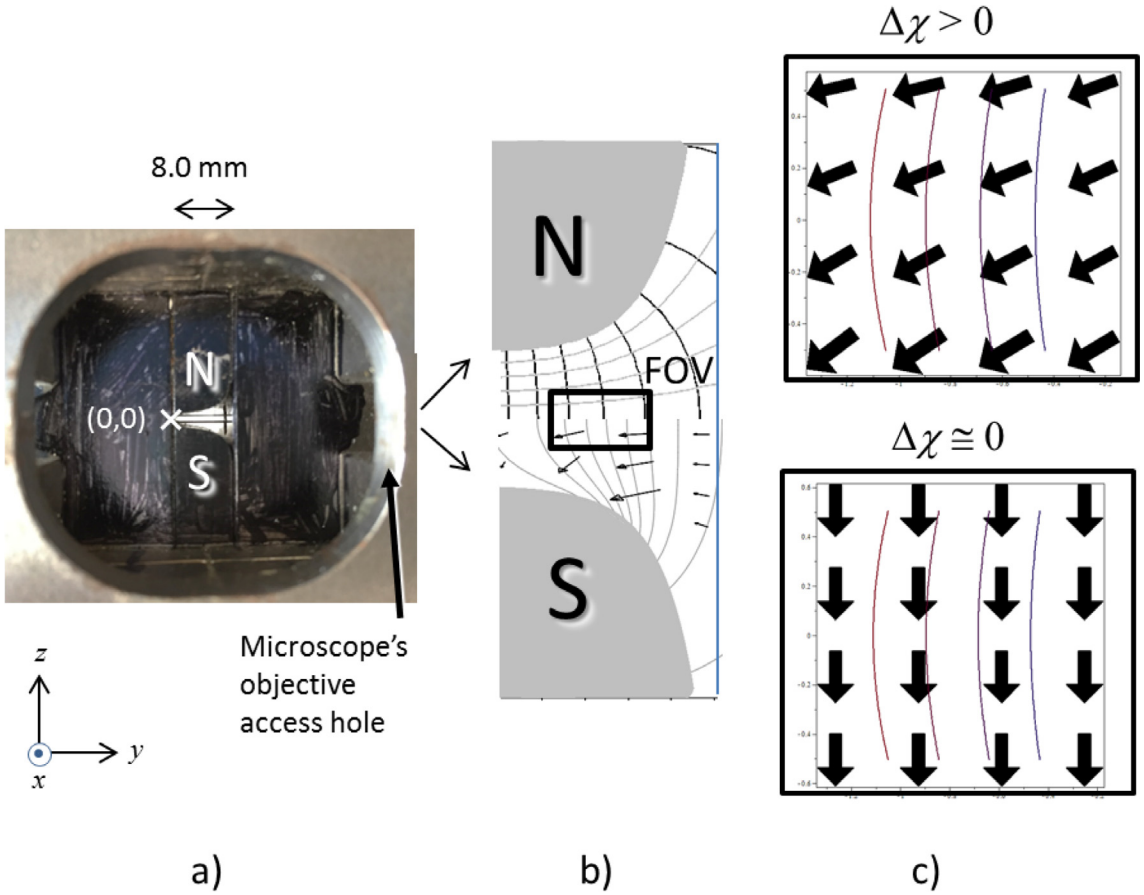

Fig. 1. Operating principle of cell magnetophoresis analyzer, by cell tracking velocimetry (CTV). a) Photograph of the portion of the permanent magnet showing glass sample holder and hyperbolic shape of the pole pieces. The microscope objective (not shown) is oriented along the *x*-axis. b) Composite diagram of the equipotential and field lines (upper half) and magnetostatic potential isolines and force vectors (lower half) of the CTV magnet. The microscope's field of view (FOV) is targeted at the magnetic field area with the least variable magnetic forces. c) Model simulation of the total velocity vectors of RBC-like objects distributed on a grid in microscope' FOV. For those objects whose magnetic susceptibility is greater than that of the medium ($\Delta\chi > 0$, deoxy- and met-RBCs, top panel) there is a magnetophoretic effect comparable in magnitude to the sedimentation effect. For $\Delta\chi \cong 0$ (oxy-RBCs, bottom panel) there is no magnetophoretic effect. The model predictions were confirmed by the experiment, Figs. 5 and 6. The magnetostatic equipotential lines are indicated by gray lines.

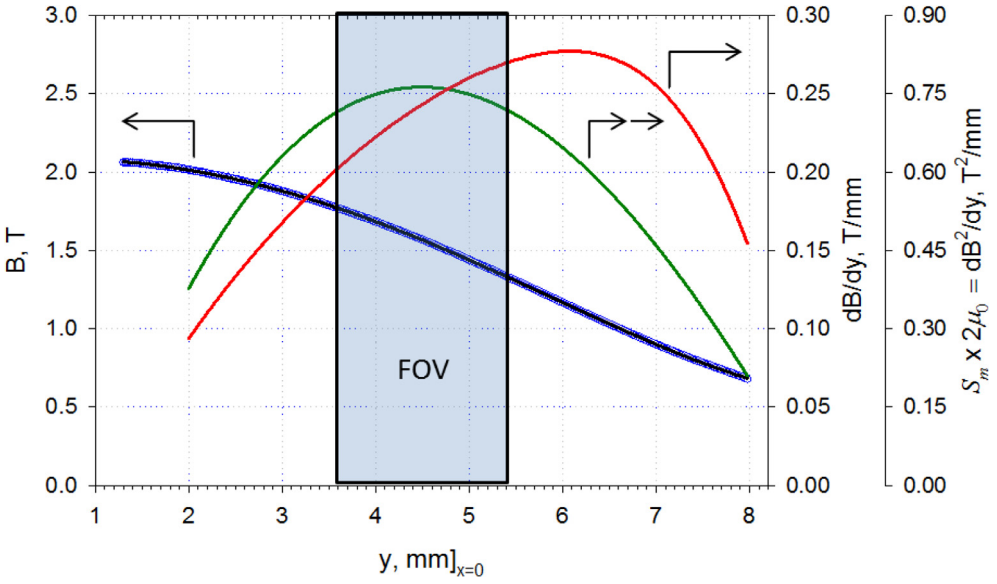

Fig. 2. Key magnetostatic field parameters determining RBC magnetophoresis: B field, the gradient of B field and twice the product of the two, dB^2/dx a quantity that is proportional to the magnetostatic potential energy gradient, S_m. Note nearly constant potential energy gradient in the field of view (FOV, shaded area), a field property sometimes referred to as "isodynamic".

(T), μ_0 is the magnetic permeability of free space ($4\pi \times 10^{-7}$ T-m/A).

Magnetophoretic analyzer also records cell velocity component orthogonal to magnetophoresis' direction, v, along the vertical z-axis (Fig. 1c), and therefore provides additional information about the cell's or fluid's property required for solving Eq. (3), from the cell sedimentation equation:

$$v = \frac{\rho_{RBC} - \rho_{H2O}}{18\pi\eta} D_{RBC}^2 g \tag{4}$$

where D_{RBC} is the cell diameter (m), ρ_{RBC} and ρ_{RBC} are the cell and fluid densities (kg/m^3). and $g = 9.81$ m/s^2 is the standard gravitational acceleration. The numerical values of quantities used to calculate RBC volume magnetic susceptibility from its magnetophoretic, u_m and v, sedimentation velocities in Eqs. (3) and (4), respectively are $\rho_{RBC} = 1125$ kg/m^3, $\rho_{H2O} = 1000$ kg/m^3, $\eta = 0.00089$ Pa.s at 25C, and $\chi_{H2O} = -9.05 \times 10^{-6}$. The average magnetostatic potential energy density gradient over FOV in Eq. (3) for Mk V magnet assembly is $S_m = 1/2\mu_0 \times 750$ T^2/m $= 2.98 \times 10^8$ T-A/m^2 (Fig. 2). The design of magnet pole pieces ensured that the magnetic force field contributed less than 2% to the standard deviation of the RBC sedimentation velocity and its effect was negligible on the mean sedimentation velocity across the FOV.

Cell suspension was held in the square glass channel of 1 mm I.D. and 1.4 mm O.D., which is placed horizontally and attached to a Hamilton valve on each end to eliminate interference flow during the measurement (Figs. 1 and 3). To accommodate the RBC deoxygenation protocol, one end of the glass channel was connected to 35 mL custom-made cylindrical deoxygenator. During the preparation of the deoxygenated RBC, the blood sample in the deoxygenator was continuously infused with humidified nitrogen, agitated by magnetic stirring bar and monitored by the dissolved oxygen probe (Fig. 3). Also two N_2 environment sheaths were attached to the channel-tubing connections to avoid re-oxygenation of the cells (Fig. 3). The motion of migrating cells was monitored through 5x objective lens (LMPlanFl, Olympus, Japan), 3.3x photo-eyepiece (U-PMTVC, Olympus, Japan), and CCD camera (Retiga 200R, QImaging, Canada). The acquired images are recorded with Video Savant software and analyzed using custom image analyzing software ImageView. The image analyzer identifies a particle by selecting threshold value on a pixel grayscale, and records it location, frame-by-frame by calculating the most probable location in the frame from the location in the preceding frame [33]. The particle velocity is calculated by linear fit of cell centroid position versus time data, for the set of frames in which a particle is tracked. This parameter is at the discretion of the user and can range from 3 to the total number of frames acquired, 50 in the case of the work described here.

Additional information about the RBC sample preparation is provided in section "2.3 RBC magnetic susceptibility by SQUID-MPMS", below. Before the measurement, the RBCs were washed with PBS then converted into different forms: 1) oxygenated blood cells, oxy RBCs: the cells were diluted with PBS to the final concentration of 5×10^5 cell/mL and kept in equilibrium with air before being infused to the channel by syringe; 2) met-hemoglobin RBC, met-RBCs: the cells were treated with 5 mM $NaNO_2$/PBS for 1 h at cell concentration of 5×10^6 cells/mL, and then washed with PBS and diluted to the final concentration of 5×10^5 cell/mL with PBS for infusion into the channel; and 3) deoxygenated RBCs, deoxy RBCs: whole blood were suspended with PBS to the final concentration of 5×10^5 cell/mL and then infused into the channel-deoxygenator system (Fig. 3). Valves were closed to prevent the exposure to air. The sample was deoxygenated for 1 h prior to the measurement.

Before recording the cell migration, the sample was left undisturbed with the valves closed for 100–200 s. The motion of cells was recorded within 50 frames and frame interval of 2 s. The valves were then opened and new cell aliquot was inserted into FOV by syringe. The valves were closed again and the recording was repeated until 10 sets of images (~1000 cell tracks) were recorded.

2.2. Measurement range of the cell magnetophoretic analysis

The magnetophoretic measurement limits are imposed by physical constraints, such as maximum field value and gradient homogeneity over FOV of the CTV apparatus, the dark field microscope diffraction limit, thermal noise floor due to Brownian motion, the creeping flow ceiling imposed by low particle Stokes number assumption, and wall effect of the channel. The additional technical constraints are imposed by the cell tracking software algorithm, including the image pixel resolution. The details are discussed below.

2.2.1. Thermal noise limit

Thermal noise causes Brownian motion of microscopic particles and introduces uncertainty as to the magnitude of single particle displacement associated with weak body forces, such as magnetic force acting on the RBC. Assuming identical diameter and magnetic susceptibility of all particles tested, a constant magnetic field energy gradient within microscope FOV, and negligible inter-particle interactions, the mean square RBC displacement over the time of observation due to thermal

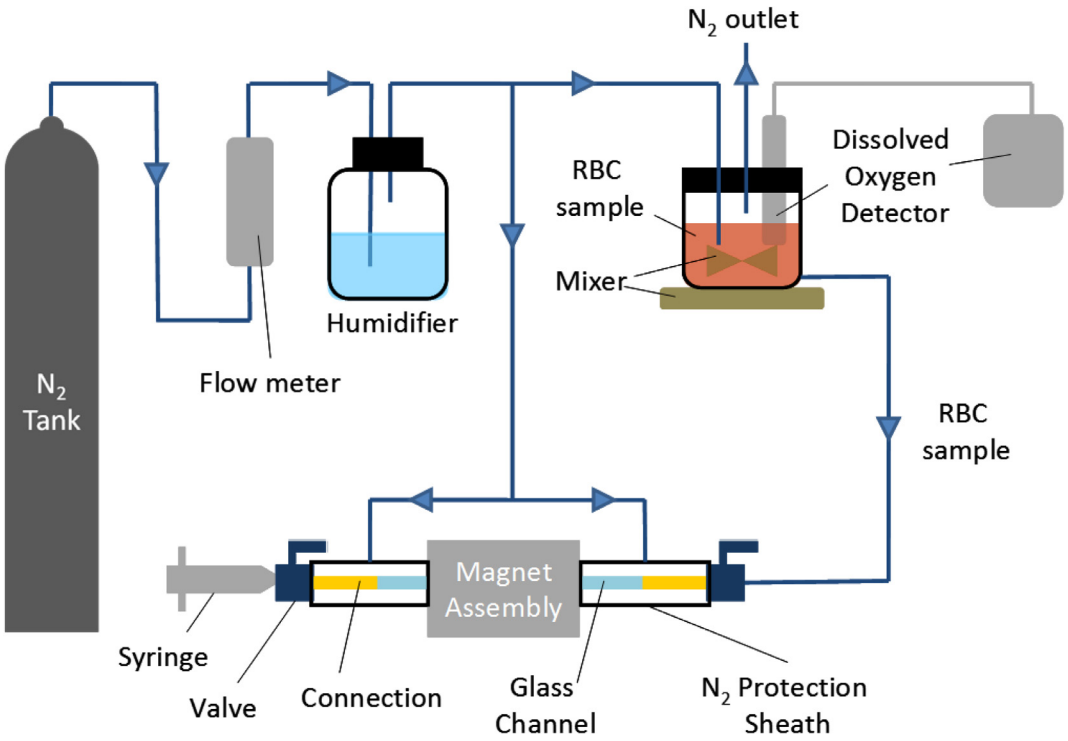

Fig. 3. Deoxygenated RBC magnetophoresis experimental setup. Note use of N_2–gas filled protective sheaths enveloping blood tubing to minimize O_2 diffusion from the atmosphere.

motion follows the Einstein equation [34]:

$$\langle x_{RBC}^2 \rangle = \frac{2k_B T}{3\pi\eta D_{RBC}} t \tag{5}$$

where k_B is the Boltzmann constant (1.38×10^{-23} $m^2 kg\ s^{-2}\ K^{-1}$), T is the absolute temperature (293 K), t is the observation time (here 100 s), η is the viscosity of water (1.00×10^{-3} Pa ·s), and D_{RBC} is the RBC hydrodynamic diameter (5.56 μm assuming mean RBC volume of 90 fL). The resulting root-mean-square displacement of a single RBC due to the Brownian motion over the time tracking is $\sqrt{\langle x^2 \rangle} = 3.9$ μm, and the resulting uncertainty of the magnetic field-induced RBC velocity is $\delta u_m = \pm \sqrt{\langle x^2 \rangle}/t = \pm 0.039$ μm/s. By substitution of δu_m into Eq. (3), the resulting error of single RBC magnetic susceptibility determination is $\delta\chi_{RBC} = \pm 1.96 \times 10^{-7}$, approximately 20% of the water magnetic susceptibility value (-0.905×10^{-6}).

The accuracy of RBC susceptibility measurement improves with the increased RBC sample size, N. For instance, the statistically detectable difference from 0 of the measured RBC magnetophoretic velocity magnitude is calculated from one-sample case formula [35]:

$$|u_m|_{\min} = \left| \frac{1.96\delta u_m}{\sqrt{N}} \right| \tag{6}$$

For a representative number of RBCs tracked of $N = 1000$ during a typical magnetophoretic analysis and $\delta u_m = \pm 0.039$ μm/s quoted above, one obtains $|u_m|_{\min} = 2.42 \times 10^{-9}$ m/s. This exceedingly small value indicates that with the current CTV technique capable of tracking thousands of RBCs per measurement, the thermal noise contribution to the error of RBC susceptibility measurement can be made negligible.

2.2.2. Creeping flow limit

Eqs. (1) and (3) hold for Stokes flow regime (creeping flow). Allowing for less than 1% relative error in the terminal RBC magnetophoretic velocity when calculated from Stokes formula for the viscous drag force imposes a maximum allowable particle Reynolds number value of not greater than 0.1 [36]. Hence we have:

$$\mathrm{Re}_{\max} = \frac{D_{RBC} \cdot |u_m|_{\max}}{\frac{\eta}{\rho}} = 0.1,$$

$$\text{therefore } |u_m|_{\max} = 0.1\frac{\eta}{\rho D_{RBC}} \tag{7}$$

where ρ is the density of water at room temperature (1×10^3 kg/m^3). The resulting $|u_m|_{\max} = 1.8$ cm/s is orders of magnitude higher than the expected RBC magnetophoretic velocity in the current apparatus. The corresponding maximum expected magnetic susceptibility of such fast moving microparticle is calculated from Eq. (3), $|\chi|_{\max} = 9.05 \times 10^{-2}$. Again, this is four orders of magnitude higher than the absolute susceptibility of water and corresponds to susceptibility of superparamagnetic microparticles [1]. Consequently, the RBC magnetophoresis is well within the limit of the creeping flow model.

2.2.3. Particle-particle interaction

According to Famularo [37] the correction of settling velocity of dilute random suspension due to inter-particle interactions is approximated by the formula:

$$\frac{u}{u_0} = \frac{1}{1 + 1.30\phi^{1/3}} \tag{8}$$

where u and u_0 are the corrected and uncorrected velocity (from the Stokes law), respectively. Parameter ϕ is the volume fraction of suspended cells. For a RBC suspension of cell number concentration of 5×10^{-5} cells/mL, the effect of particle-particle interaction lowers the mean migration velocity by 4.5% relative to that, calculated from the Stokes law.

2.2.4. Wall effect

The foregoing discussion of the Stokes drag is applicable to particles moving in an infinite volume of the viscous fluid. Yet in the RBC magnetophoresis experiment the cells are typically suspended in a long, parallel-piped glass channel of 1 mm × 1 mm cross section (Fig. 1) which introduces deviation from Stokes drag due to the finite cell diameter, here D_{RBC} (5.56 μm), especially near the walls of the square cross section channel. We approximate the resulting fractional

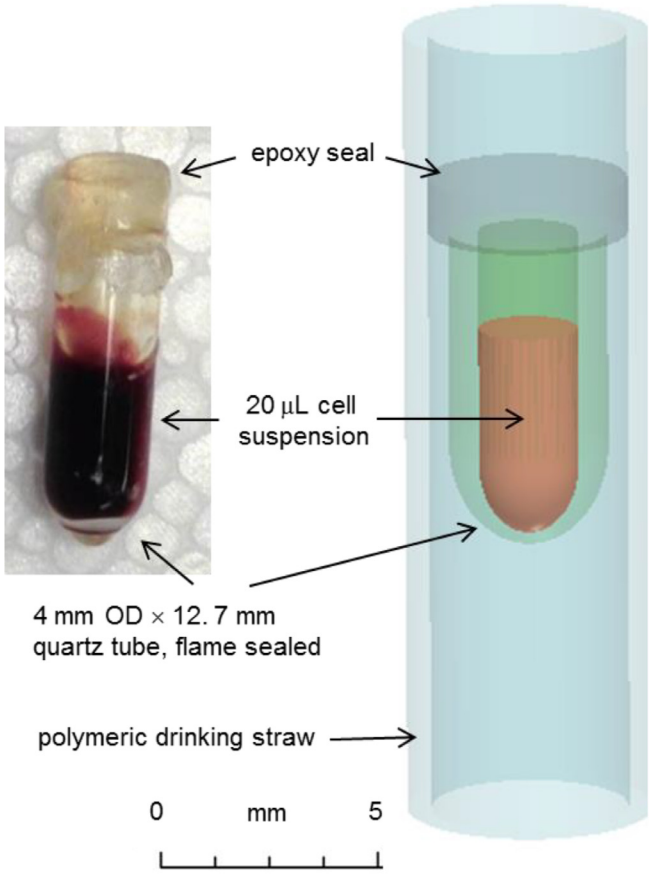

Fig. 4. Blood sample container for SQUID-MPMS red blood cell magnetic susceptibility determination. Right panel illustrates placement of the container in the SQUID-MPMS apparatus.

deviation of the actual cell velocity from the Stokes velocity, $\frac{\delta u}{u}$ by using Happel and Bart's work [38] for the sphere settling along the axis of a square duct of the wall width l, at low Reynolds's number:

$$\frac{\delta u}{u} = 1.903266\frac{D_{RBC}}{l} = 0.011 \quad (9)$$

The deviation is just above 1% and therefore the wall effects were neglected in the magnetophoretic RBC susceptibility analysis.

2.2.5. Image resolution and light diffraction limit

In dark-field microscopy used for cell tracking, the minimum trackable particle size is around 200 nm according to Rayleigh criterion. Furthermore, the image resolution of current magnetophoresis system is limited to 1.53 μm/pixel. Particles smaller than that are considered not trackable. Note that if the particle is fluorescent, the minimum trackable size could be lower [39].

2.2.6. Image analyzer algorithm

The maximum tractable velocity by the image analyzer is determined by the maximum particle displacement between two consecutive frames and the minimum frame time interval. To ensure the accuracy of finding one particular particle, the maximum displacement of one particle between 2 consecutive frames is set as 1/10 of the frame width. With current resolution of 1200 × 500 pixels (set with consideration of uniformity of S_m, and the analysis throughput) and aforementioned 1.53 μm/pixel spatial resolution, the maximum displacement is 184 μm. Furthermore, the minimum frame time interval is limited by data transition rate from the camera to the PC, which is 5 frames/s at current settings. The resulting upper velocity limit is 918 μm/s. Combined with Eq. (3), we obtain the relation between maximum susceptibility difference and the particle diameter.

It is worth mentioning a few ways of increasing the maximum measurable susceptibility difference, including switching to a magnet assembly with smaller S_m parameter, increasing the viscosity of liquid (e.g. by adding glycerol), increasing liquid magnetic susceptibility (e.g. by adding Gd^{3+} ions), and increasing the binning of the image, which essentially lowers the quality of the image and increase the number of frames transferred in given time. As for the minimum velocity, it could be lowered by increasing the frame time interval to such length that the particle migrates for 1 pixel distance, which may approach the thermal noise limit and become impractically lengthy.

2.3. RBC magnetic susceptibility by SQUID-MPMS

The SQUID MPMS-5 (Quantum Design, San Diego, USA) located in the Physics Department of The Ohio State University was used in this study as a benchmark for RBC susceptibility data obtained by magnetophoretic analysis. The centerpiece of SQUID-MPMS system is rf-SQUID, which is a sensitive magnetometer (flux-to-voltage converter) based on the Josephson's tunneling effect [40] and magnetic flux quantization [41]. Rather than directly interacting with the rf-SQUID, the sample interacts with the signal pick-up loop, which is a superconducting second-order gradiometer used to eliminate signal drift. A superconducting magnet magnetizes the sample, considered a point-mass, at a wide range of the applied field (up to −8 T to +8 T) and at a precisely controlled temperature. The SQUID-MPMS system was equipped with the Reciprocating Sample Option (RSO) tool that moves the sample (guided by a generic polymer drinking straw) in a reciprocal motion at multiple sampling points along the gradiometer axis thus inducing current in the gradiometer coils, proportional to the sample magnetic moment. Repeated measurements improve the accuracy of the method.

Blood samples were purchased from American Red Cross, Columbus, OH or Cleveland Clinic Pathology Department (following approval of the respective institutional ethics review boards) then washed with phosphate buffer saline (PBS) followed by RBC count, and treated for hemoglobin conversion into three different forms differing in the magnetic susceptibility, as follows:

1) The conversion to diamagnetic hemoglobin was achieved by exposing the RBC aliquot to air and sealing the RBC sample in the quartz tube for SQUID-MPMS analysis in the air atmosphere.
2) The conversion to paramagnetic met-hemoglobin was achieved by treating RBC aliquot with 5 mM $NaNO_2$ for 1 h, followed by transfer to a quartz glass container, as described below.
3) The conversion to paramagnetic deoxygenated hemoglobin was achieved by spreading 2 mL RBC aliquot in 57 cm^2 Petri dish and placing the dish inside a sealed glove box filled with 90% N_2 and 10% H_2 gas for 1 h. The subsequent transfer of the deoxyRBC sample to a sealed SQUID-MPMS sample holder was performed inside the same glove box. Twenty μL RBC aliquot was transferred to a container of 12.7 mm in length, formed from a quartz tubing O.D. 4 mm by flame-sealing one end in the glass-blowing laboratory, OSU, prior to the experiment. The other end was sealed with epoxy resin in the glove box container and cured for 1 h (Fig. 4). The sealed tubes were tested in vacuum for 1 h to ensure that they were airtight. The samples were affixed to a polymeric drinking straw and taken for the SQUID-MPMS measurement. All measurements were taken at 300 K (pre-equilibrated) and the applied field range from −70,000 Oe to 70,000 Oe (500 Oe step-size, 29 sampling points in total). As all the parts of the sample and holder assembly contribute to the SQUID-MPMS signal, the contribution from the constituent sample holder, liquid media, air and nitrogen atmosphere were determined independently of the RBC sample measurement. The total volume magnetization of the RBC sample-holder assembly is the volume-

weighed mean of its constituents, including the cells, the suspending media (PBS), the quartz tube, the gas in the tube and the epoxy seal. Therefore, the RBC contribution was calculated as the difference between the SQUID-MPMS signal, s and the other constituents:

$$\chi_{RBC} = \frac{s - \sum_{i=1}^{k} \chi_i V_i - \sum_{j=1}^{l} \chi'_j W_j}{V_{RBC}} \quad \text{where } s = \frac{\langle \Delta m \rangle}{\langle \Delta H \rangle} \tag{10}$$

and s is the slope of the experimentally determined regression line of m on H (emu/Oe). The SQUID-MPMS measurements were reported in CGS system of units. Here H is the applied field strength (Oe), m is the total magnetic moment of the sample at applied field H (emu), m_i is the magnetic moment of constituent i at the applied field H (emu), χ_i is the volume magnetic susceptibility of constituent i (dimensionless), V_i is the volume of constituent i (cm^3), χ'_j is the mass magnetic susceptibility of constituent j (cm^3/g), W_j is the mass of constituent j (g). By knowing the value of all terms except the magnetic susceptibility of RBC, χ_{RBC} in Eq. (3), the mean volume magnetic susceptibility of the RBC in suspension was calculated. The error of the SQUID-MPMS method was calculated by error propagation. The numerical value of the magnetic susceptibility in CGS system is converted to that in SI units system by multiplying by 4π.

2.4. Theory and calculations

RBC volume magnetic susceptibility was calculated from susceptibilities of its components, including hemoglobin with oxygen-saturated heme groups (oxy RBC, null magnetic moment contribution from O_2-heme group), hemoglobin without oxygen (deoxy RBC, 4 Bohr magnetons per heme group), and hemoglobin with covalently bound oxygen to the heme groups, or methemoglobin, met RBC (5 Bohr magnetons per heme group) [42,43]. The model was described in detail elsewhere [14]. The values of net volume RBC magnetic susceptibility, first entry in Table 1 therein, denoting difference between susceptibilities of RBC and water (in CGS units system), $\Delta\chi_{RBC} = \chi_{RBC} - \chi_{H2O} = -0.0147 \times 10^{-6}$ (oxy RBC), 0.265×10^{-6} (deoxy RBC), and 0.301×10^{-6} (met RBC) were used to calculate the RBC susceptibility by adding that of water and multiplying by 4π for conversion to the SI units system, resulting in $\chi_{RBC} = -9.23 \times 10^{-6}$ (oxy RBC), -5.72×10^{-6} (deoxy RBC), and -5.27×10^{-6} (met RBC).

2.5. Error analysis

The magnetophoretic and sedimentation velocity distributions did not meet the criteria of random distributions (by Shapiro-Wilk normality test at p less than 0.05) and therefore Mann-Whitney rank sum test was used for testing for difference between means. Statistical analysis software package SigmaPlot© v.14 from Systat Software, Inc. was used for data analysis and graphical presentation. The sources of error are discussed in preceding section "2.2 Measurement range of the cell magnetophoretic analysis". The resulting uncertainty in the cell velocity determination are estimated at 0.3 μm/s on average over the entire range of the velocity values. An important source of velocity data dispersion is the natural size distribution of RBCs. The RBC volume coefficient of variation is 28% (by Coulter Counter, data not shown). An important part of the magnetophoretic velocity determination is achieving a steady state cell motion. This was accomplished by adding a wait time of 100 s to 200 s after the sample injection into the channel before commencing the image acquisition.

The sources of error in the proposed method of SQUID-MPMS measurement of liquid blood sample is mainly related to the fact that the cells contribute only a small portion to the total magnetic moment of the sample and container volume (estimated at less than 10%). The cell count uncertainty in the sample (by hemacytometer) is approximately 10%. Additional sources of error include deviation from the point mass assumption of the sample and holder assembly and heterogeneity of the cell suspension [44,45]. Less than 3% error is introduced if the volume of the sample is not larger than 5% of the gradiometer volume, assuming that it is properly aligned with the centerline of the gradiometer and the RSO approach is used, applicable to our technique. A common source of error in both methods of the RBC susceptibility determination is the uncertainty in the completeness of RBC de-oxygenation, which is difficult to achieve because of high affinity of hemoglobin to oxygen at low oxygen concentration.

3. Results and discussion

The RBC magnetophoretic and sedimentation velocity distributions for all three types of hemoglobin are shown in Fig. 5 (single species RBCs) and Fig. 6 (oxy RBC mixed in equal proportion with met RBCs). The mean RBC volume magnetic susceptibilities calculated from their mean magnetophoretic velocities using Eqs. (3) and (4) are shown in Table 1. Also included in the Table are SQUID-MPMS results and theoretical values calculated from known concentration of intracellular hemoglobin, magnetic moment of hemoglobin compounds of deoxygenated, oxygenated and oxidized (met) hemoglobin, RBC volume and its equivalent spherical RBC diameter and fluid media viscosity [14]. Inspection of Fig. 5a shows clear separation of magnetophoretic peaks between oxy RBC and met RBC samples (highly significant by Mann-Whitney test at $p < 0.001$). The same, clear separation of peaks is observed for oxy RBC and deoxy RBC samples, Fig. 5b. The oxy Hb mean magnetophoretic velocity was small and negative as expected of a particle that is slightly more diamagnetic than water (the 99% confidence interval of the mean, $[-0.1, -0.06]$ μm/s, did not contain the null value). In contrast, no significant difference was detected between deoxy RBC and met RBC magnetophoretic velocity distributions (Fig. 5a and b).

The sedimentation velocity distributions are comparable for all three RBC species, with overlapping peaks and negligible differences between respective mean velocities compared to the unity standard deviation (Fig. 5 and Table 1). This is expected of the RBC samples differing only in their oxygen binding status. However, the corresponding mean RBC equivalent spherical diameters, D_{RBC} calculated from Eq. (4), are significantly larger, 9.8–10.2 μm than expected for normal RBCs from healthy individuals, 5.6 μm (equivalent spherical

Table 1
Volume magnetic susceptibility (SI) of RBC measured by magnetophoresis (mean ± SD, sample sizes as shown in Figs. 5 and 6) and compared to SQUID-MPMS (mean ± standard error) and from theoretical calculations [14]. Value of $\chi_{H2O} = -9.05 \times 10^{-6}$ was used for water.

Method	Parameter	Oxy RBC	Deoxy RBC	Met RBC
Magnetophoresis	v (μm/s)	2.31 ± 0.36	2.39 ± 0.57	2.55 ± 0.41
	D_{RBC} (μm)	9.8 ± 3.8	9.9 ± 5.0	10.2 ± 4.1
	u_m (μm/s)	−0.08 ± 0.26	1.55 ± 0.66	1.61 ± 0.55
	$\chi_{RBC} \times 10^6$	−9.19 ± 0.47	−6.39 ± 1.1	−6.46 ± 0.88
SQUID-MPMS	$\chi_{RBC} \times 10^6$	−9.73 ± 1.34	−7.34 ± 1.17	−6.02 ± 1.1
Theory	$\chi_{RBC} \times 10^6$ (CGS)	−0.7349	−0.4552	−0.4192
	$\chi_{RBC} \times 10^6$	−9.23	−5.72	−5.27

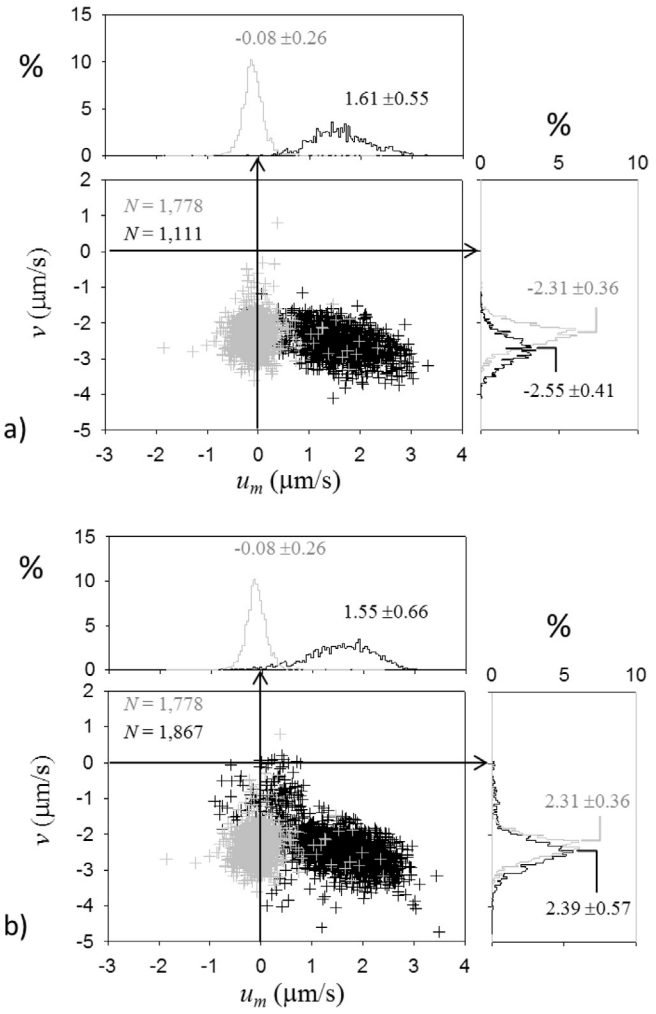

Fig. 5. Single population RBC magnetophoretic velocity (horizontal axis) and sedimentation velocity (vertical axis) scatter plots with the respective marginal histograms. Oxygenated RBCs are shown in gray. a) Methemoglobin RBCs. b) Deoxygenated RBCs. Note shift in the RBC magnetophoretic velocity distributions from low to high values with the conversion of low spin Hb (oxy RBC) to high spin Hb (methemoglobin or deoxy RBC, black). The sedimentation velocity of the three types of RBCs remained unchanged (side histograms), as expected. The size of the cross marks approximates two mean standard deviations of a single track RBC velocity measurement. Parameter N denotes number of RBCs tracked, and 102 bins were used for constructing each histogram.

diameter of a 90 fL normocyte). The reason for the difference compared to the normal value is unclear and could be related to the discoid shape of the RBC leading to its faster sedimentation than expected from the RBC equivalent spherical diameter calculated by standard reference methods (cell electrical impedance measurement used in Coulter counter or by cell image analysis). An intriguing possibility is a spatial ordering of RBCs by the imposed magnetic field known for orienting the RBCs with their disk plane along the B field lines (note the nearly vertical direction of B field lines in the microscope FOV shown in Fig. 1c) [46]. This would significantly decrease the RBC retardation by the fluid frictional forces as the RBC falls in the fluid edge-on.

Another potential source of discrepancy is the type of blood used in the study (stored blood rather than freshly collected). Nevertheless, when used for calculation of the RBC susceptibility from Eq. (3), the measured RBC diameters result in the RBC susceptibility values that are within the experimental error of SQUID-MPMS results and are comparable to those calculated from theory, Table 1. Significantly, the oxy RBC susceptibility is lower than that of water and the deoxy RBC and met RBC susceptibilities are higher compared to water, as expected

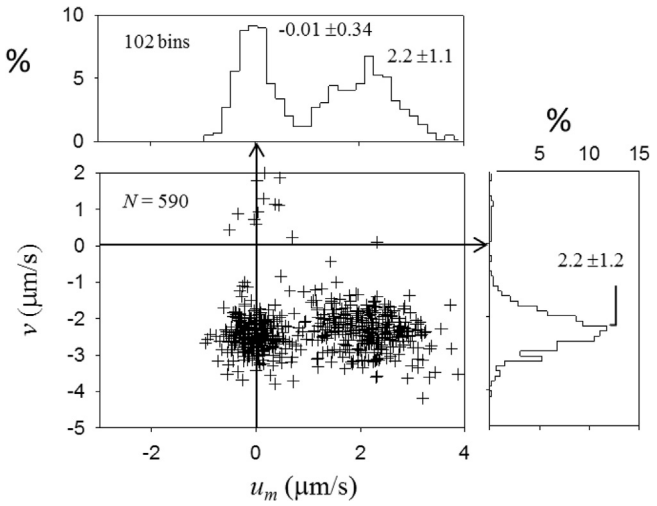

Fig. 6. As in Fig. 5 but for a 50:50 mixture of oxy RBCs and met RBCs in suspension. Note clear segregation of the sample into two populations with respect to the RBC magnetophoretic velocity but not the sedimentation velocity, as expected from the results for single RBC populations shown in Fig. 5.

from the theory, Table 1. Those differences are highly significant, based on significant separation of magnetophoretic velocity peaks in Fig. 5, and the significant shift of the oxy RBC magnetophoretic velocity peak to negative side of the null value, discussed above. Again, no difference was measured between deoxy RBC and met RBC values by magnetophoresis, although comparatively higher values are expected for met RBC from the theory and indeed, are so measured by SQUID-MPMS, Table 1. Interestingly, the SQUID-MPMS values were systematically lower than the corresponding values obtained by RBC magnetophoresis, and lower than expected from theory. This could be related to a systematic error introduced by a large diamagnetic contribution from fused silica/quartz sample tube ($\chi = -11.3 \times 10^{-6}$) as compared to a relatively small cell contribution, and possibly by the cell number undercount.

Significantly, the magnetophoretic velocity distribution for a mixed population of oxy RBCs and met RBCs, Fig. 6 correctly reproduced the peaks seen for the separately analyzed RBC populations, Fig. 5. Simultaneous measurement of component susceptibilities in a mixture was not possible by the SQUID-MPMS method.

SQUID-MPMS was used before to determine magnetic properties of biological matter but not in its native state, as used in our work. In particular, Hackett et al. [27] examined the iron susceptibility in various form of hemoglobin including oxyhemoglobin, methemoglobin and hemoglobin from malaria-infected RBCs by measuring the susceptibility of frozen RBC lysate in SQUID-MPMS at 10 K and 265 K and showed a positive correlation between the iron susceptibility from malaria-infected RBCs and the maturation of malaria parasite. Karl et al. [4] measured the magnetic properties of lympholyzed Schistosome eggshells (*S. mansoni* and *S. japonicum*) from 10 to 300 K that suggested presence of a mixture of high and low spin iron in the sample. Mejias et al. [28] examined the magnetic nanoparticle uptake by tissue in lympholized samples at 10–100 K and showed decreasing susceptibility over time indicating degradation of the particles. Hashimoto [47] developed a paper-strip adhesion method to measure the concentration of magnetic particles attached to cell surface. Our work demonstrated that with proper attention to finding the right sample container (such as fashioned from a quartz tubing), careful sealing (to avoid He gas contamination inside the SQUID-MPMS used to control the temperature) and proper calibraion of all the sample holder components, the SQUID-MPMS could be also used for liquid sample measurements.

Magnetophoretic cell analysis used in this work is a part of a large

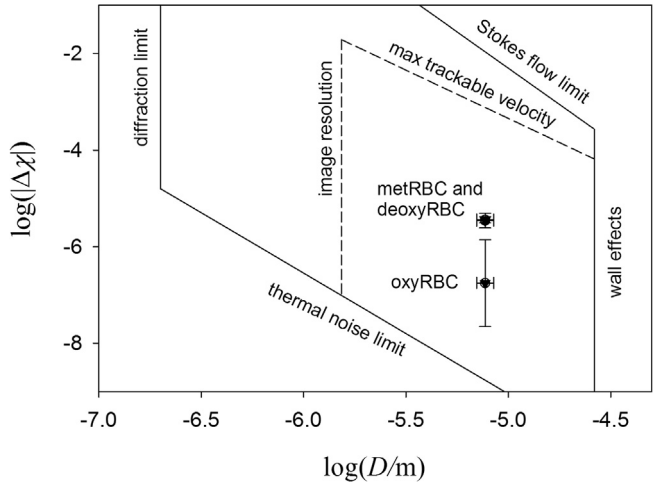

Fig. 7. Limits of CTV magnetophoretic analysis related to particle diameter, D, and its net volume magnetic susceptibility relative to fluid, $\Delta\chi$. Solid line represents absolute limits and the dashed line represents the limits of the current system. The result for oxygenated RBCs (oxyRBC), methemoglobin RBCs (metRBC) and deoxygenated RBCs (deoxy) are also shown (together with their population standard deviations at $N \approx 1000$).

family of magnetophoretic methods developed for analytical and preparative applications in biomedical research and laboratory medicine. Relevant examples include already cited work by Watarai et al. [7] later modified to include zero-velocity approach using susceptibility gradient in the liquid media for improved accuracy [30]. "Thales" system was developed for specialized applications to characterization of 1–10 μm particles requiring lower magnetic field and gradient than used in this work [3]. Mair and Superfine [31] used magnetophoresis to study interactions between magnetic nanorods and extracellular matrix. The unique feature of the magnetophoretic method used in this study it the extension of a nearly constant magneto-ponderomotive force acting on a cell, S_m over the entire microscope's FOV (Fig. 2). This increases the accuracy of the cell magnetophoretic velocity measurement and makes it a useful parameter for magnetic susceptibility calculation. The added feature of a (nearly) orthogonal cell sedimentation velocity measurement provides means for calculation of an equivalent spherical diameter of the cell (providing that its density is also known). The simultaneous measurement of the cell magnetophoretic, u_m and sedimentation, v velocities provides a means to eliminate the cell diameter altogether from the cell susceptibility calculation by working with the ratio of the two, u_m/v (note how D_{RBC} cancels out when working with Eqs. (1) and (4); incidentally, the fluid viscosity, η cancels out, too). The measurement range of the magnetophoretic method is summarized in Fig. 7. We continue testing the method's capability in applications to measuring cell susceptibility in its natural milieu.

4. Conclusions

Cell magnetophoresis in a well-defined magnetostatic potential energy gradient, coupled with microscopic cell motion analysis provides unique means of an intact, single cell magnetic susceptibility measurement in its minimally modified milieu (physiologic electrolyte solution). The accuracy of the method was tested on human red blood cells differing in hemoglobin type known for difference in the magnetic susceptibility: diamagnetic oxy-hemoglobin, paramagnetic deoxy-hemoglobin and met-hemoglobin. The RBC population mean values agreed, within the experimental error, with the susceptibility measurements performed by SQUID-MPMS, used as a reference standard, for all three different RBC species, thus establishing cell magnetophoresis determination by CTV as a viable method of single cell susceptometry. Based on a number of cells required for measurement and considering that at least 5000 RBCs were required for a meaningful SQUID-MPMS measurement, the CTV susceptometry is estimated to be 5000 times more sensitive than SQUID-MPMS. This was confirmed for a mixed RBC population containing both diamagnetic and paramagnetic hemoglobin species producing bimodal RBC magnetophoretic velocity distribution with well-separated peaks, at peak locations corresponding to single species measurements, a result unattainable by SQUID-MPMS. Current work concentrates on further increase in sensitivity of the magnetophoretic analysis to further test the method on other cell types known for the presence of paramagnetic constituents [48].

Acknowledgment

We thankfully acknowledge technical support of Boris Kligman. This research was supported by the National Institutes of Health award number R01CA062349 and R01HL131720. Support for N.N. was provided by Cleveland Clinic – Mie University Research Exchange Program (Profs. Takashi Horiuchi and Masahiro Tomita, Directors).

References

[1] N.T.K. Thanh, Clinical Applications of Magnetic Nanoparticles, CRC Press, Boca Raton, FL, 2018.
[2] A. Buck, L.R. Moore, C.D. Lane, A. Kumar, C. Stroff, N. White, W. Xue, J.J. Chalmers, M. Zborowski, Magnetic separation of algae genetically modified for increased intracellular iron uptake, J. Magn. Magn. Mater. 380 (2015) 201–204.
[3] S.L. Hackett, T.G. St Pierre, Thales: an instrument to measure the low field magnetophoretic mobility of microscopic objects, J. Phys. Conf. Ser. 17 (2005) 181–184.
[4] S. Karl, L. Gutierrez, R. Lucyk-Maurer, R. Kerr, R.R.F. Candido, S.Q. Toh, M. Saunders, J.A. Shaw, A. Suvorova, A. Hofmann, M.J. House, R.C. Woodward, C. Graeff-Teixera, T.G. St Pierre, M.K. Jones, The iron distribution and magnetic properties of schistosome eggshells: implications for improved diagnostics, Plos Neglect Trop D 7 (2013).
[5] P. Quentin, J. Stephen, D. Jon, Applications of magnetic nanoparticles in biomedicine: the story so far, J. Phys. D: Appl. Phys. 49 (2016) 501002.
[6] M. Zborowski, J.J. Chalmers, Magnetic cell manipulation and sorting, in: W. Lee, P. Tseng, D. Di Carlo (Eds.), Microtechnology for cell manipulation and sorting, Springer International Publishing, Cham, Switzerland, 2017.
[7] H. Watarai, M. Namba, Capillary magnetophoresis of human blood cells and their magnetophoretic trapping in a flow system, J. Chromatogr. A 961 (2002) 3–8.
[8] P.A. Zimmerman, J.M. Thomson, H. Fujioka, W.E. Collins, M. Zborowski, Diagnosis of malaria by magnetic deposition microscopy, Am. J. Trop. Med. Hyg. 74 (2006) 568–572.
[9] S. Karl, M. David, L. Moore, B.T. Grimberg, P. Michon, I. Mueller, M. Zborowski, P.A. Zimmerman, Enhanced detection of gametocytes by magnetic deposition microscopy predicts higher potential for Plasmodium falciparum transmission, Malar. J. 7 (2008) 66.
[10] K. Melnik, J. Sun, A. Fleischman, S. Roy, M. Zborowski, J.J. Chalmers, Quantification of magnetic susceptibility in several strains of Bacillus spores: implications for separation and detection, Biotechnol. Bioeng. 98 (2007) 186–192.
[11] J. Sun, M. Zborowski, J.J. Chalmers, Quantification of both the presence, and oxidation state, of Mn in Bacillus atrophaeus spores and its imparting of magnetic susceptibility to the spores, Biotechnol. Bioeng. 108 (2011) 1119–1129.
[12] X. Jin, S. Abbot, X. Zhang, L. Kang, V. Voskinarian-Berse, R. Zhao, M.V. Kameneva, L.R. Moore, J.J. Chalmers, M. Zborowski, Erythrocyte enrichment in hematopoietic progenitor cell cultures based on magnetic susceptibility of the hemoglobin, PloS One 7 (2012) e39491.
[13] L.R. Moore, F. Nehl, J. Dorn, J.J. Chalmers, M. Zborowski, Open gradient magnetic red blood cell sorter evaluation on model cell mixtures, IEEE Trans. Magn. 49 (2013) 309–315.
[14] M. Zborowski, G.R. Ostera, L.R. Moore, S. Milliron, J.J. Chalmers, A.N. Schechter, Red blood cell magnetophoresis, Biophys. J. 84 (2003) 2638–2645.
[15] X. Jin, M.H. Yazer, J.J. Chalmers, M. Zborowski, Quantification of changes in oxygen release from red blood cells as a function of age based on magnetic susceptibility measurements, The Analyst 136 (2011) 2996–3003.
[16] X. Jin, Y. Zhao, A. Richardson, L. Moore, P.S. Williams, M. Zborowski, J.J. Chalmers, Differences in magnetically induced motion of diamagnetic, paramagnetic, and superparamagnetic microparticles detected by cell tracking velocimetry, Analyst 133 (2008) 1767–1775.
[17] K.A. Mirica, S.T. Phillips, C.R. Mace, G.M. Whitesides, Magnetic levitation in the analysis of foods and water, J. Agric. Food. Chem. 58 (2010) 6565–6569.
[18] K.A. Mirica, S.T. Phillips, S.S. Shevkoplyas, G.M. Whitesides, Using magnetic levitation to distinguish atomic-level differences in chemical composition of polymers, and to monitor chemical reactions on solid supports, J. Am. Chem. Soc. 130 (2008) 17678–17680.
[19] S. Ge, Y. Wang, N.J. Deshler, D.J. Preston, G.M. Whitesides, High-throughput density measurement using magnetic levitation, J. Am. Chem. Soc. (2018).
[20] T. Savas, A.K. Joseph, C.T. Huseyin, T. Clemence, E.K. Antoine, C.G. Ionita,

D. Utkan, Levitational image cytometry with temporal resolution, Adv. Mater. 27 (2015) 3901–3908.
[21] N.N. Greenwood, R. Greatrex, Mössbauer spectroscopy, (2007).
[22] J.K.M. Sanders, B.K. Hunter, Modern NMR Spectroscopy: A Guide for Chemists, Oxford University Press, Oxford; New York, 1989.
[23] N.M. Atherton, M. Davies, B. Gilbert, Electron Spin Resonance, Royal Society of Chemistry, 1996.
[24] C.J. Oconnor, Magnetochemistry – advances in theory and experimentation, Prog. Inorg. Chem. 29 (1982) 203–283.
[25] S. Foner, Citation classic – versatile and sensitive vibrating-sample magnetometer, Cc/Eng. Tech. Appl. Sci. (1985) 14.
[26] E.M. Haacke, R.W. Brown, M.R. Thompson, R. Venkatesan, Magnetic resonance imaging, Phys. Principles Sequence Des. (1999).
[27] S. Hackett, J. Hamzah, T.M.E. Davis, T.G. St Pierre, Magnetic susceptibility of iron in malaria-infected red blood cells, BBA-Mol. Basis Dis. 1792 (2009) 93–99.
[28] R. Mejias, L. Gutierrez, G. Salas, S. Perez-Yague, T.M. Zotes, F.J. Lazaro, M.P. Morales, D.F. Barber, Long term biotransformation and toxicity of di-mercaptosuccinic acid-coated magnetic nanoparticles support their use in biomedical applications, J. Control. Release 171 (2013) 225–233.
[29] E.P. Furlani, Magnetophoretic separation of blood cells at the microscale, J. Phys. D Appl. Phys. 40 (2007) 1313–1319.
[30] H. Watarai, H.T.T. Duc, T.T.N. Lan, T.Y. Zhang, S. Tsukahara, Zero-velocity magnetophoretic method for the determination of particle magnetic susceptibility, Anal. Sci. 30 (2014) 745–749.
[31] L.O. Mair, R. Superfine, Single particle tracking reveals biphasic transport during nanorod magnetophoresis through extracellular matrix, Soft Matter. 10 (2014) 4118–4125.
[32] E.L. Persons, STUDIES ON RED BLOOD CELL DIAMETER: III. The relative diameter of immature (reticulocytes) and adult red blood cells in health and anemia, especially in pernicious anemia, J. Clin. Invest. 7 (1929) 615–629.
[33] J.J. Chalmers, S. Haam, Y. Zhao, K. McCloskey, L. Moore, M. Zborowski, P.S. Williams, Quantification of cellular properties from external fields and resulting induced velocity: magnetic susceptibility, Biotechnol. Bioeng. 64 (1999) 519–526.
[34] A. Einstein, Investigations on the Theory of the Brownian Movement, Courier, Dover Publications, 1956.
[35] G. van Belle, Statistical Rules of Thumb, Second, Edition ed., John Wley & Sons Inc, Hoboken, NJ, 2008.
[36] M. Rhodes, Introduction to particle technology, 1998, in, Wiley & Sons.
[37] J. Happel, H. Brenner, Low Reynolds number hydrodynamics: with special applications to particulate media, Springer, 1983.
[38] J. Happel, E. Bart, The settling of a sphere along the axis of a long square duct at low Reynolds' number, Appl. Sci. Res. 29 (1974) 241–258.
[39] J. Xu, K. Mahajan, W. Xue, J.O. Winter, M. Zborowski, J.J. Chalmers, Simultaneous, single particle, magnetization and size measurements of micron sized, magnetic particles, J. Magn. Magn. Mater. 324 (2012) 4189–4199.
[40] B.D. Josephson, Possible new effects in superconductive tunnelling, Phys. Lett. 1 (1962) 251–253.
[41] B.S. Deaver, W.M. Fairbank, Experimental evidence for quantized flux in superconducting cylinders, Phys. Rev. Lett. 7 (1961) 43–46.
[42] L. Pauling, C.D. Coryell, The magnetic properties and structure of hemoglobin, oxyhemoglobin and carbonmonoxyhemoglobin, Proc. Nat. Acad. Sci. U.S.A. 22 (1936) 210–216.
[43] L. Pauling, C.D. Coryell, The magnetic properties and structure of the hemochromogens and related substances, Proc. Nat. Acad. Sci. U.S.A. 22 (1936) 159–163.
[44] P. Stamenov, J. Coey, Sample size, position, and structure effects on magnetization measurements using second-order gradiometer pickup coils, Rev. Sci. Inst. 77 (2006) 015106.
[45] M. Sawicki, W. Stefanowicz, A. Ney, Sensitive SQUID magnetometry for studying nanomagnetism, Semicond. Sci. Technol. 26 (2011) 064006.
[46] T. Higashi, A. Yamagishi, T. Takeuchi, N. Kawaguchi, S. Sagawa, S. Onishi, M. Date, Orientation of erythrocytes in a strong static magnetic field, Blood 82 (1993) 1328–1334.
[47] S. Hashimoto, T. Oda, K. Yamada, M. Takagi, T. Enomoto, N. Ohkohchi, T. Takagi, T. Kanamori, H. Ikeda, H. Yanagihara, E. Kita, A. Tasaki, The measurement of small magnetic signals from magnetic nanoparticles attached to the cell surface and surrounding living cells using a general-purpose SQUID magnetometer, Phys. Med. Biol. 54 (2009) 2571–2583.
[48] J.J. Chalmers, X. Jin, A.F. Palmer, M.H. Yazer, L. Moore, P. Amaya, K. Park, X. Pan, M. Zborowski, Femtogram Resolution of iron content on a per cell basis: ex vivo storage of human red blood cells leads to loss of hemoglobin, Anal. Chem. 89 (2017) 3702–3709.